

## Magnetic Excitations in Uranium Dioxide

R. A. COWLEY AND G. DOLLING

*Chalk River Nuclear Laboratories, Chalk River, Ontario, Canada*

(Received 28 August 1967)

The spin-wave dispersion relations have been measured in antiferromagnetic uranium dioxide by inelastic neutron-scattering techniques. The triple-axis crystal spectrometer at the C5 facility of NRU was used throughout in its constant-Q mode of operation. The dispersion relations were obtained for spin waves propagating along the main symmetry directions at 9°K, and less complete measurements were made at higher temperatures both above and below the Néel temperature. The theory of spin waves in UO<sub>2</sub> is developed and various models are used in attempts to deduce the exchange and anisotropy parameters from the experimental results. None of the models are completely satisfactory, because of the difficulties arising from the multidomain character of the specimen, and from the strong interaction between the magnons and the phonons. A theory of this interaction is also developed which gives quite reasonable agreement with experiment.

### I. INTRODUCTION

THE spin-wave dispersion relations of several materials have now been studied by means of inelastic scattering of slow neutrons from single-crystal specimens. For example, the acoustic and optic spin waves of ferrimagnetic magnetite were determined by Watanabe and Brockhouse<sup>1</sup> and the dispersion relation of antiferromagnetic manganese fluoride was observed by Okazaki, Turberfield, and Stevenson.<sup>2</sup> This paper reports similar measurements on antiferromagnetic uranium dioxide. Uranium dioxide has the fluorite structure in the paramagnetic phase. [Each ion is situated on a face-centered cubic lattice, and if the uranium is taken at the origin of the unit cell, the oxygen ions are at  $(\frac{1}{4}, \frac{1}{4}, \frac{1}{4})a$  and  $(-\frac{1}{4}, -\frac{1}{4}, -\frac{1}{4})a$ .] The dispersion relations of the normal modes of the atomic vibrations in the paramagnetic phase have been reported in an earlier publication.<sup>3</sup> Below 30.8°K, the material is antiferromagnetic. The magnetic structure<sup>4-6</sup> is shown in Fig. 1. The ferromagnetic sheets are perpendicular to a(001) axis, and the magnetic moments are known to lie within the sheets, although their exact direction is unknown. No change in ionic structure at the transition has as yet been reported.

The studies of the spin-wave dispersion relations of magnetite and of manganese fluoride showed that the magnetic interactions could be described accurately by a model including the effects of Heisenberg forces between near-neighbor ions and weak single-ion anisotropy fields. Uranium dioxide, however, is almost certainly more complex, because in contrast to these other cases, the magnetic moment does not arise wholly from the spin of the electrons.

Measurements of the magnetic form factor<sup>5,6</sup> suggest that the electronic configuration of the magnetic electrons is  $(5f)^2$ . In the  $L$ - $S$  coupling approximation, the ground state is then  ${}^3H_4$ , which is further perturbed by the octahedral crystalline field. Point-charge calculations<sup>7,8</sup> suggest that the lowest level will be either a  $\Gamma_1$  singlet or a  $\Gamma_{25}'$  triplet. The magnetic properties of UO<sub>2</sub> can then be expected to be different from those of magnetite and manganese fluoride, because the ions do not have a spherically symmetric orbital configuration. Furthermore, Blume<sup>9</sup> has suggested that the  $\Gamma_1$  singlet is also of very low energy and is responsible for the unusual abruptness of the transition.<sup>6</sup>

In the next section, the experiment and the results are described. The magnetic excitations have been determined along high symmetry directions at 9°K by inelastic scattering of slow neutrons. A restricted set of experiments is also described to determine the temperature dependence of the magnetic excitations, especially in the region of the transition temperature. The theory of spin waves in UO<sub>2</sub> is described in Sec. III. The main difficulty in interpreting the experimental results in terms of the theory arises because of the domain structure present in the specimen. Since UO<sub>2</sub> is cubic in its paramagnetic phase, each of the three  $\langle 001 \rangle$  axes are equally likely to be perpendicular to the ferromagnetic sheets.

The experiments show striking examples of the interaction between the phonons and the magnetic excitations, as previously reported.<sup>10</sup> This interaction considerably complicates the analysis of the experimental results, and it appears to be very difficult to obtain a completely consistent and comprehensive picture of the system. Analyses of the experimental results by means of conventional spin-wave theory in two different ways are described in Sec. IV, and compared with Allen's theory of the spin waves in UO<sub>2</sub>.<sup>11</sup>

<sup>1</sup> B. N. Brockhouse and H. Watanabe, in *Inelastic Scattering of Neutrons in Solids and Liquids* (International Atomic Energy Agency, Vienna, 1963), Vol. II, p. 297.

<sup>2</sup> A. Okazaki, K. C. Turberfield, and R. W. H. Stevenson, *Phys. Letters* **8**, 9 (1964).

<sup>3</sup> G. Dolling, A. D. B. Woods, and R. A. Cowley, *Can. J. Phys.* **43**, 1397 (1965).

<sup>4</sup> D. G. Henshaw and B. N. Brockhouse, *Bull. Am. Phys. Soc.* **2**, 9 (1957).

<sup>5</sup> B. T. M. Willis and R. J. Taylor, *Phys. Letters* **17**, 188 (1965).

<sup>6</sup> B. C. Frazer, G. Shirane, D. E. Cox, and C. E. Olsen, *Phys. Rev.* **140**, A1449 (1965).

<sup>7</sup> C. A. Hutchinson and G. A. Candela, *J. Chem. Phys.* **27**, 707 (1957).

<sup>8</sup> H. U. Rahman and W. A. Runciman, *J. Phys. Chem. Solids* **27**, 1833 (1966).

<sup>9</sup> M. Blume, *Phys. Rev.* **141**, 517 (1966).

<sup>10</sup> G. Dolling and R. A. Cowley, *Phys. Rev. Letters* **16**, 683 (1966).

<sup>11</sup> S. J. Allen, *J. Appl. Phys.* **38**, 1479 (1967).

A theory of the magnon-phonon interaction is introduced in Sec. V and, with the aid of the models of the phonon spectra deduced earlier,<sup>3</sup> and of models deduced for the magnon spectra, it is shown to give reasonable agreement with experiment. The large magnon-phonon interaction arises because the distortion of the lattice due to the presence of a phonon is able to split the triplet ground state. In magnetic materials with an orbital singlet for a ground state, the crystalline field is not able to split the ground state, and there is correspondingly only a weak magnon-phonon interaction, as found in magnetite and manganese fluoride, for example.

Finally, in Sec. VI, the results of the previous sections are summarized, and a brief mention is made of the mechanism of the antiferromagnetic phase transition in  $\text{UO}_2$ . It is hoped to give a detailed account of the theory of this transition, together with calculations of the temperature dependence of the magnon spectrum and related properties in a future publication.

## II. EXPERIMENT

### 1. Experiment Details

The single-crystal specimen of uranium dioxide was of cylindrical shape, approximately 2 cm in diameter and 4 cm long, with a  $\langle 111 \rangle$  axis along the length of the cylinder. It was selected from a large quantity of fused uranium dioxide and then heated with hyperstoichiometric uranium dioxide to a temperature of  $1900^\circ\text{K}$  in a stream of hydrogen to improve the stoichiometry. (We are indebted to R. L. Stoute for assistance in preparing the specimen.) The mosaic spread was  $0.3^\circ$ . The initial set of experiments<sup>3</sup> were conducted with a crystal kindly given to us by H. J. Anderson of General Electric Company, Richland, Washington.

The specimen was oriented with the  $[1\bar{1}0]$  axis vertical, and placed in a metal helium cryostat. The crystal was surrounded by a radiation shield which was supported from the helium bath above by a thin-walled stainless steel spacer, and the whole arrangement was

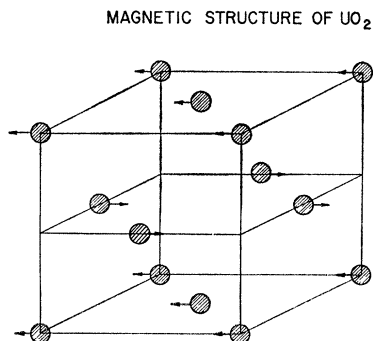


FIG. 1. Magnetic structure of  $\text{UO}_2$  below  $30.8^\circ\text{K}$ . Only the uranium ions are shown. Their magnetic moments lie in planes parallel to the cube faces of the paramagnetic phase, but the direction of these moments is otherwise unknown.

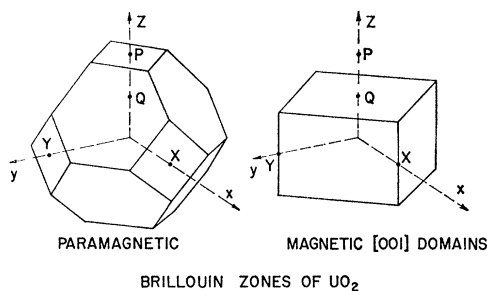


FIG. 2. Brillouin zones of paramagnetic and antiferromagnetic  $\text{UO}_2$ .

surrounded by a radiation shield in good thermal contact with the helium bath. Temperatures close to the Néel temperature were obtained with the aid of an electrical heater placed near the specimen. The temperature was monitored with a germanium resistance thermometer and was stable to  $0.1^\circ\text{K}$  for periods as long as a week.

The experiments were performed with the triple-axis crystal spectrometer at the NRU reactor.<sup>12</sup> The constant- $Q$  technique was used throughout, with scattered neutron energies 18.26 and 15.16 meV for most of the experiments. The experiments consisted in recording scattered neutron energy distributions for certain selected momentum transfers. The center of each neutron group then yields the frequency  $\nu(j)$  of the excitation of preselected momentum  $\mathbf{q}$  simply by application of the equations of conservation of energy and momentum.

### 2. Reciprocal Lattice

The Brillouin zone of the magnetically ordered and paramagnetic phases of uranium dioxide differ (see Fig. 2). In Fig. 3, the reciprocal-lattice points and Brillouin-zone boundaries in the  $(1\bar{1}0)$  plane are shown for both phases. In the antiferromagnetic phase, the zones are complicated by the domain structure of the crystal. The ferromagnetic sheets may be aligned perpendicular to any of the three mutually perpendicular  $\langle 001 \rangle$  axes, and the orientation of the Brillouin zone differs for the different domains. The additional reciprocal-lattice points  $(h, k, l)$  associated with the  $[001]$  domains are given by

- (a)  $h+k$  even  
 (b)  $h+l$  odd.

Consequently, the only additional reciprocal-lattice points to occur in the  $(1\bar{1}0)$  plane arise from the  $[001]$  domains. These domains and also those of the  $[100]$  and  $[010]$  domains are shown in Fig. 3.

In view of the different zones for the different domains, there is the possibility of ambiguity in assigning experimental results to particular domains. Conse-

<sup>12</sup> B. N. Brockhouse, in *Inelastic Scattering of Neutrons in Solids and Liquids* (International Atomic Energy Agency, Vienna, 1961), p. 113.

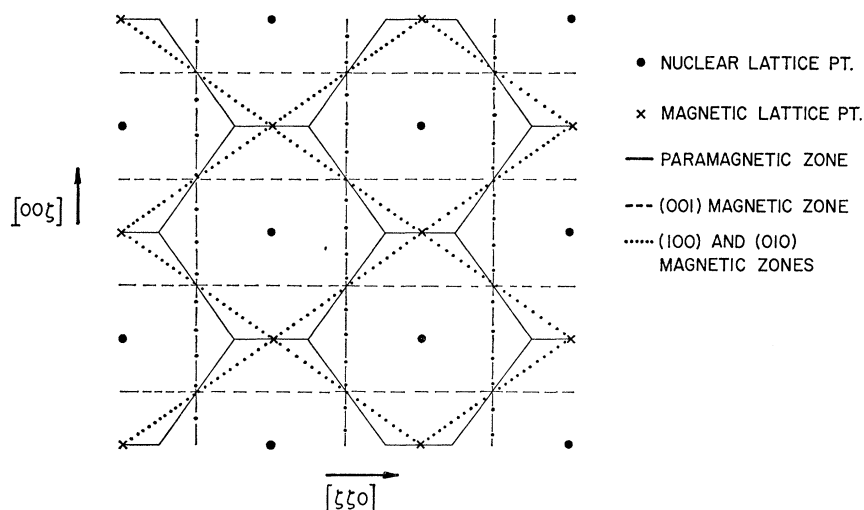
$(\bar{1}\bar{1}0)$  PLANE RECIPROCAL LATTICE OF ANTIFERROMAGNETIC  $\text{UO}_2$ 

FIG. 3.  $(110)$  plane sections through the Brillouin zones shown in Fig. 2. The filled circles and solid lines represent reciprocal lattice points and zone boundaries for the paramagnetic phase, while the crosses and dashed curves represent these quantities in the magnetic phase, assuming  $(001)$ -type domains. The zone boundaries for the  $(010)$ - and  $(100)$ -type domains are shown as dotted lines (their reciprocal lattice points lie outside the plane of this figure).

quently, the measurements are presented using the wave vectors of the paramagnetic Brillouin zone, and are then not subject to such possible errors of interpretation. The assignment of the measurements to different domains will be discussed in Sec. IV.

### 3. Experimental Results at $9^\circ\text{K}$

The experimental results at  $9^\circ\text{K}$  are shown in Fig. 4 for the low-frequency excitations propagating along the high symmetry directions  $[00\xi]$ ,  $[\xi\xi 0]$ ,  $[\xi\xi\xi]$ , and  $[\xi\xi 1-\xi]$ . The measurements along  $[\xi\xi\xi]$  were actually performed at  $4.6^\circ\text{K}$ , but there was no detectable change in frequency between  $4.6$  and  $9^\circ\text{K}$ . Some of the frequencies at high symmetry points are listed in Table I. Also shown in Fig. 4 are the phonon-dispersion curves, calculated using model III of Dolling *et al.*<sup>3</sup> Since this model was obtained by fitting its parameters to give agreement with  $296^\circ\text{K}$  results, they do not yield the phonon-dispersion curves at  $9^\circ\text{K}$  accurately. Nevertheless they do provide a fairly reliable guide to the shape and approximate locations of the latter curves.

It is of interest to compare the frequencies observed here with those obtained by far-infrared techniques. Daniel<sup>13</sup> has observed two absorption lines at frequencies of  $2.955$  and  $2.34$ , whereas, more recently, Allen<sup>11</sup> and Aring and Sievers<sup>14</sup> have observed additional weaker lines at  $0.54$  and  $0.69$ , of which the former is split by a magnetic field whereas the latter is probably an impurity level. These frequencies are in good agreement with our frequencies at  $q=0$  and  $\mathbf{q}=(0, 0, 1)a/2\pi$ .

Unfortunately, in the case of uranium dioxide, it is

not possible to distinguish readily between the neutron groups obtained from scattering by phonons and those obtained from magnetic excitations, using unpolarized neutron beams. It is very difficult to change the direction of magnetization, while the magnetic form factor decreases so slowly with neutron momentum transfer that the phonons cannot easily be observed in a region where the magnetic intensity is negligible. The only possible way of distinguishing them is by a careful analysis of the intensities for different positions in reciprocal space which have the same reduced wave vectors. However the effects of double-scattering processes<sup>15</sup> may invalidate even this approach.

### 4. Temperature Dependence

The temperature dependence of some of the excitations has also been observed near the magnetic transition temperature, which was determined to be  $30.5 \pm$

TABLE I. The frequency ( $10^{12}$  cps) of some low-lying excitations in  $\text{UO}_2$  at  $9^\circ\text{K}$ . The wave vectors are in units of  $(2\pi/a)$ .

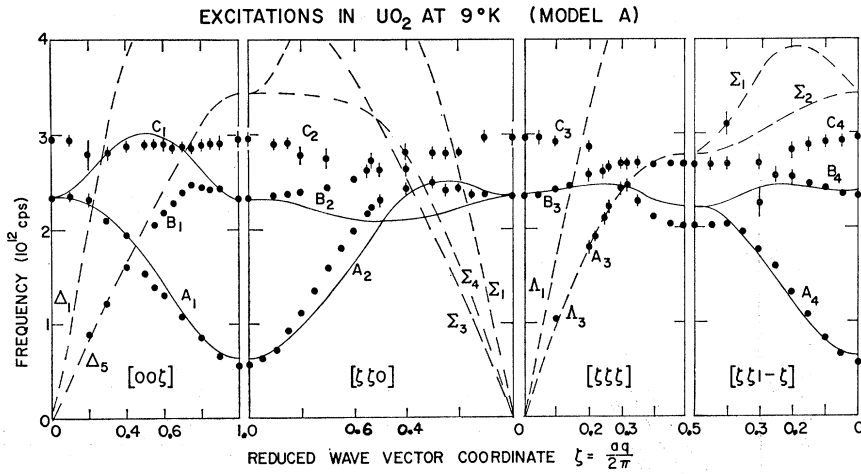
Wave vector	Frequency
$(0, 0, 0)$	$2.34 \pm 0.03$
	$2.96 \pm 0.05$
$(0, 0, 1)$	$0.57 \pm 0.01$
	$2.33 \pm 0.025$
	$2.96 \pm 0.04$
$(0.5, 0.5, 0.5)$	$2.03 \pm 0.02$
	$2.68 \pm 0.03$

<sup>13</sup> M. R. Daniel, Phys. Letters **22**, 131 (1966).

<sup>14</sup> K. Aring and A. J. Sievers, J. Appl. Phys. **38**, 1467 (1967).

<sup>15</sup> G. Dolling and A. D. B. Woods, in *Thermal Neutron Scattering*, edited by P. A. Egelstaff (Academic Press Inc., New York, 1965), Chap. V, p. 206.

FIG. 4. The measured dispersion relation for excitations in  $\text{UO}_2$  at  $9^\circ\text{K}$ , propagating along four directions in the crystal. The dashed curves show the phonon-dispersion curves appropriate to  $296^\circ\text{K}$ . The solid curves are the result of a least-squares fitting procedure in which the experimental measurements are assigned labels according to model AB (see Sec. IV).



$0.5^\circ\text{K}$  for our specimen. In particular, measurements were made of the lowest frequency branch in the  $[\xi\xi 1-\xi]$  direction and of the modes with wave vectors  $(0, 0, 0)$ ,  $(0, 0, 1) \times 2\pi/a$ , and  $(0.9, 0.9, 0) \times 2\pi/a$ . In Fig. 5, some of the neutron groups obtained for three of these modes are shown, while in Fig. 6 the temperature dependence of the  $[\xi\xi 1-\xi]$  branch of the lowest frequency is shown. The experimental resolution was insufficient to separate, at every temperature, the magnetic Bragg reflection from the neutron

groups corresponding to the lowest frequency mode at  $(0, 0, 1) \times 2\pi/a$ . Nevertheless, it is clear that this frequency approaches zero at the transition temperature, as shown in Fig. 7. The temperature dependence of the intensity of a magnetic Bragg reflection is also shown for comparison.

The results shown in Fig. 5 demonstrate that as the Néel temperature is approached the intensity of the peaks decrease, the intensity of the background increases, and the peak positions decrease in frequency

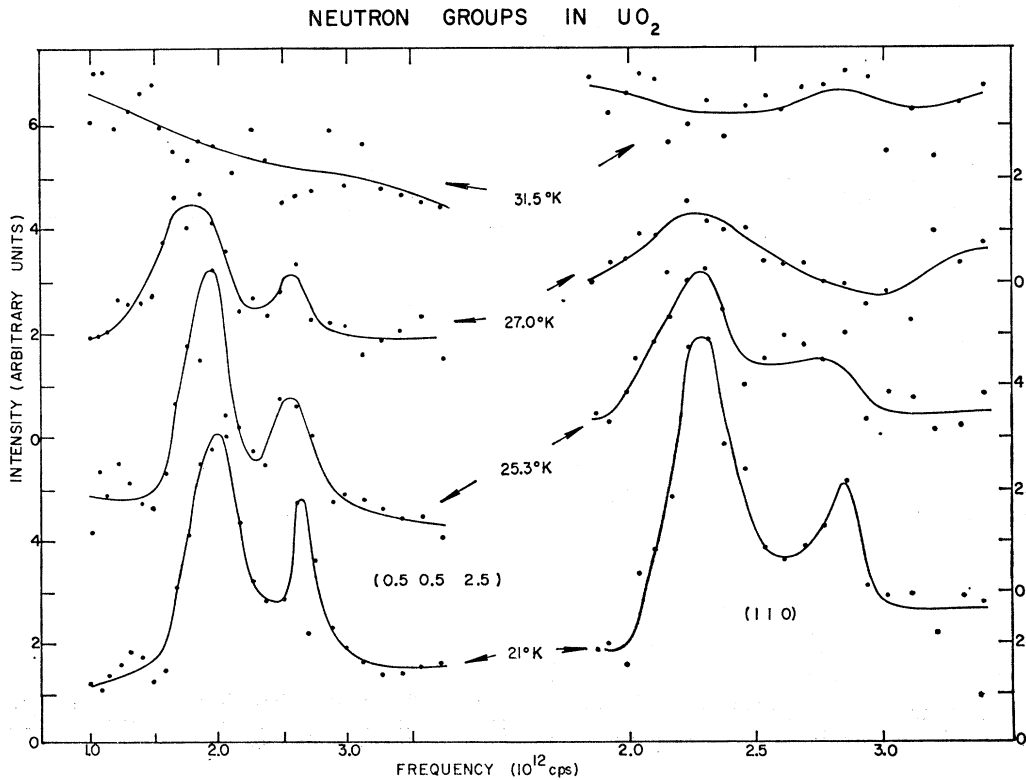


FIG. 5. Neutron groups observed at various temperatures in experiments corresponding to two reduced wave vectors.

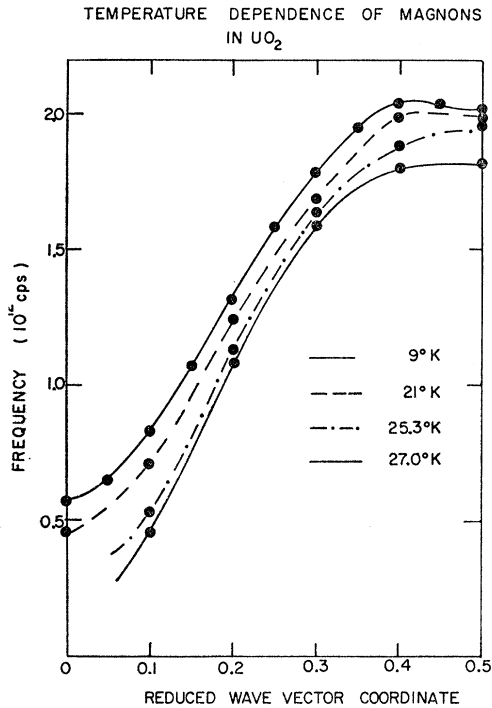


FIG. 6. Temperature dependence of the  $[\xi\xi 1-\xi]$  branch of lowest frequency.

a little, as shown also in Table II. The decrease in intensity is particularly apparent for the high-frequency upper branches, but not so marked for the lower. A rather surprising result is that there was little increase in the width of the peaks below  $T_N$ . This behavior is to be compared with that of manganese fluoride, as measured by Turberfield *et al.*,<sup>16</sup> for which the spin waves become very broad well below the Néel temperature.

### III. SPIN-WAVE THEORY

#### 1. Electronic Structure of $U^{4+}$

The measurements of the magnetic form factor of  $U^{4+}$  ions by Willis and Taylor<sup>6</sup> and by Frazer *et al.*<sup>6</sup> suggest that the configuration of the magnetic electrons is  $(5f)^2$ . In the actinide series, the spin-orbit coupling is stronger than the crystal field, so the ground state is a  $^3H_4$  configuration. In an octahedral cubic crystalline field, this configuration is split into four states: a singlet  $\Gamma_1$ , a doublet  $\Gamma_{12}$ , and two triplets,  $\Gamma_{15}'$  and  $\Gamma_{25}'$ . Point-charge calculations show that the ground state may be either the  $\Gamma_1$  or  $\Gamma_{25}'$  states.<sup>7</sup> The more careful calculations of Rahman and Runciman,<sup>8</sup> however, suggest that  $\Gamma_{25}'$  is the ground state. This is in agreement with the magnitude of the specific-heat anomaly as meas-

ured by Jones *et al.*<sup>17</sup> when the phonon contribution to the specific heat is calculated using the measured phonon-dispersion relations.<sup>3</sup>

Blume's theory<sup>9</sup> of the magnetic properties of uranium dioxide requires the  $\Gamma_1$  and  $\Gamma_{25}'$  states to be of very similar energy. We shall briefly discuss the applicability of this theory to  $UO_2$  in Sec. VI, and until then we assume the ground state to be the  $\Gamma_{25}'$  triplet.

It is useful to introduce an effective spin Hamiltonian with  $S=1$  to describe the excitations within the  $\Gamma_{25}'$  triplet. Within this manifold both the spin operators and orbital angular-momentum operators of the  $U^{4+}$  ion are proportional to the effective spin operators. The proportionality constants are  $2.5(g-1)$  and  $2.5(2-g)$ , respectively, where  $g$  is the Landé splitting factor, which for  $U^{4+}$  is 0.8.

#### 2. Spin-Wave Excitations

The spin waves are the excitations of the system within the triplet ground state of the paramagnetic phase. These can be described by the effective  $S=1$  spin Hamiltonian, which, when the spin direction is taken along  $[001]$ , can be written as

$$H = -\frac{1}{2} \sum_{\langle ij \rangle} J(ij) \mathbf{S}_i \cdot \mathbf{S}_j - K_1 \sum_i (S_i^z)^2 - K_2 \sum_i [(S_i^x)^2 - (S_i^y)^2], \quad (3.1)$$

where  $J(ij)$  is a Heisenberg exchange interaction between neighboring spins  $i$  and  $j$ , and  $K_1$  and  $K_2$  are single-ion anisotropy constants. The ferromagnetic sheets are taken to be perpendicular to  $[100]$ . Strictly speaking, the spin direction within the ferromagnetic sheets is unknown, but the results for the frequencies of the spin waves are not dependent on the spin direction, so we will assume the spins to lie along the  $[001]$  crystallographic axis of the crystal. The neutron-scatter-

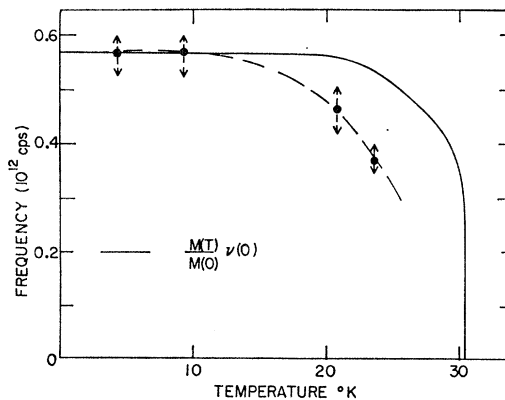


FIG. 7. Temperature dependence of the lowest frequency mode of excitation at  $q=(0,0,1)$  ( $a/2\pi$ ) compared with that of the intensity of a magnetic Bragg reflection.

<sup>16</sup> K. C. Turberfield, A. Okazaki, and R. W. H. Stevenson, Proc. Phys. Soc. (London) **85**, 1 (1965).

<sup>17</sup> W. M. Jones, J. Gordon, and E. A. Long, J. Chem. Phys. **20**, 695 (1952).

ing cross section of the spin waves is dependent on the spin direction but, in a multidomain specimen, the results again become largely independent of the spin direction.

The frequencies of the spin waves may be deduced from the Hamiltonian (3.1) by use of the Holstein-Primakoff transformation, as described by Walker,<sup>18</sup> for example. The details are given in the Appendix. For a wave vector  $\mathbf{q}$ , there are two modes whose frequencies are given by

$$\begin{aligned} \hbar\omega_1(\mathbf{q}) &= [A^2 - (B+C)^2]^{1/2} \\ \text{and} \\ \hbar\omega_2(\mathbf{q}) &= [A^2 - (C-B)^2]^{1/2}. \end{aligned} \quad (3.2)$$

The coefficients  $A$ ,  $B$ , and  $C$  are given by the exchange and anisotropy constants and depend on the wave vector  $\mathbf{q}$ . For exchange interactions between nearest- and next-nearest-neighbor ions, the expressions are

$$\begin{aligned} A &= 4SJ_1[1 - \cos(\pi\zeta_y) \cos(\pi\zeta_z)] - 4SJ_2 - 4SJ_3 \\ &\quad + 2SJ_4[1 - \cos(2\pi\zeta_x)] + 2SJ_5[1 - \cos(2\pi\zeta_y)] \\ &\quad + 2SJ_6[1 \cos(2\pi\zeta_z)] + 2K_1S, \\ B &= -SK_2, \\ C &= -4SJ_2 \cos(\pi\zeta_x) \cos(\pi\zeta_y) - 4SJ_3 \cos(\pi\zeta_x) \cos(\pi\zeta_z), \end{aligned} \quad (3.3)$$

where the reduced wave vector  $\zeta = a\mathbf{q}/2\pi$ .  $J_1$ ,  $J_2$  and  $J_3$  are the exchange constants between nearest neighbors at  $(0, \frac{1}{2}, \frac{1}{2})$ ,  $(\frac{1}{2}, \frac{1}{2}, 0)$ , and  $(\frac{1}{2}, 0, \frac{1}{2})$ , while  $J_4$ ,  $J_5$ ,  $J_6$  are between next-nearest neighbors at  $(100)$ ,  $(010)$ , and  $(001)$ , respectively.

The stability of the magnetic structure can be discussed as described by Bertaut.<sup>19</sup> If the spin direction is along  $[001]$ , then  $K_1 > |K_2|$ . The condition for the

stability of the  $[100]$  structure against small changes of the propagation vector of the structure leads to the conditions

$$-J_2 - J_3 + 2J_4 > 0, \quad (3.4)$$

$$J_1 - J_2 + 2J_5 > 0, \quad (3.5)$$

$$J_1 - J_3 + 2J_6 > 0. \quad (3.6)$$

Molecular-field theory can be used to obtain expressions for the transition temperature  $T_N$  and Curie temperature  $\theta$ . The results are

$$k_B T_N = \rho(4J_1 - 4J_2 - 4J_3 + 2J_4 + 2J_5 + 2J_6), \quad (3.7)$$

and

$$k_B \theta = \rho(4J_1 + 4J_2 + 4J_3 + 2J_4 + 2J_5 + 2J_6), \quad (3.8)$$

where

$$\rho = \frac{1}{3}S(S+1).$$

### 3. Neutron Scattering Cross Section

The cross section for scattering of neutrons by a magnetic system is discussed in detail by de Gennes.<sup>20</sup> In general, for a system with both orbital and spin angular momentum, the result is very complex; however, for small momentum transfers  $\mathbf{Q}$ , the cross section is dependent on the total angular momentum of the system  $\mathbf{J}$ . If the energy transfer to the neutron is  $\hbar\Omega$ , the differential-scattering cross section is

$$\begin{aligned} & (|\mathbf{k}| / |\mathbf{k}_0|) |(\gamma e^2 / 2mc^2) g f(\mathbf{Q})|^2 \\ & \times \sum_{nm} p_n [\langle n | \sum_i \mathbf{J}_\perp \exp(-i\mathbf{Q} \cdot \mathbf{r}_i) | m \rangle] \\ & \times [\langle m | \sum_i \mathbf{J}_\perp \exp(i\mathbf{Q} \cdot \mathbf{r}_i) | n \rangle] \delta[(E_n - E_m) / \hbar - \Omega], \end{aligned} \quad (3.9)$$

where  $\mathbf{k}$  and  $\mathbf{k}_0$  are the scattered and incident wave vectors of the neutron,  $\gamma$  is the neutron magnetic moment in nuclear magnetons ( $\gamma = 1.91$ ),  $f(\mathbf{Q})$  is the form factor of the ions, and  $\mathbf{J}_\perp$  is the component of  $\mathbf{J}$  perpendicular to  $\mathbf{Q}$ . The initial state of the crystal is labelled  $n$  and has probability  $p_n$  and energy  $E_n$ , and the final state is denoted by  $m$ . The operator  $\mathbf{J}_\perp$  can be written in terms of the effective  $S=1$  operators  $\mathbf{J}_\perp = \frac{2}{3}\mathbf{S}_\perp$ . Then, for magnon scattering, the difference in energy between the initial and final states is given by  $\hbar\omega_j(\mathbf{q})$ , and the intensity is proportional to a reduced structure factor given by

$$|\langle \sum_i \mathbf{S}_\perp^i \exp(-i\mathbf{Q} \cdot \mathbf{r}_i) \rangle|^2. \quad (3.10)$$

This expression can be evaluated with the help of the Holstein-Primakoff transformation and the spin-wave coordinates. In order to eliminate the dependence of  $\mathbf{S}_\perp$  on the wave vector  $\mathbf{Q}$ , let us consider the expression (3.10). It is fairly readily shown for our model of  $\text{UO}_2$

TABLE II. The temperature dependence of some of the magnetic modes in  $\text{UO}_2$ . The frequencies are in units of  $10^{12}$  cps and wave vectors in units of  $(2\pi/a)$ . The modes marked  $-$  were not detected while those marked  $\times$  were not studied.

Temperature (°K)	(0.5, 0.5, 2.5)	(0.9, 0.9, 1.1)	(1, 1, 0)
9	2.02±0.03		2.34±0.03
	2.67±0.03	0.83±0.02	2.95±0.05
21	2.00±0.04	0.71±0.03	2.31±0.04
	2.66±0.04		2.93±0.04
25.3	1.95±0.05	0.53±0.03	2.28±0.04
	2.51±0.06		2.72±0.04
27.0	1.75±0.05	0.46±0.03	2.26±0.06
	-		-
29.5	1.50±0.07	×	×
	-		-

<sup>18</sup> L. R. Walker, in *Magnetism*, edited by G. T. Rado and H. Suhl (Academic Press Inc., New York, 1963), Vol. I, p. 299.

<sup>19</sup> E. F. Bertaut, in *Magnetism*, edited by G. T. Rado and H. Suhl (Academic Press Inc., New York, 1963), Vol. III, p. 150.

<sup>20</sup> P. G. de Gennes, in *Magnetism*, edited by G. T. Rado and H. Suhl (Academic Press Inc., New York, 1963), Vol. III, p. 115.

TABLE III. The transformations for converting the measured wave vectors into the wave vectors appropriate for a single-domain ( $X, Z$ ) crystal.

Domain	Direction of measurement			
	$[00\zeta]$	$[\zeta\zeta 0]$	$[\zeta\zeta\zeta]$	$[\zeta\zeta 1-\zeta]$
$(x, z)$	$[00\zeta]$	$[\zeta\zeta 0]$	$[\zeta\zeta\zeta]$	$[\zeta\zeta 1-\zeta]$
$(x, y)$	$[0\zeta 0]$	$[\zeta 0\zeta]$	$[\zeta\zeta\zeta]$	$[\zeta\zeta 1-\zeta\zeta]$
$(y, z)$	$[00\zeta]$	$[\zeta\zeta 0]$	$[\zeta\zeta\zeta]$	$[\zeta\zeta 1-\zeta]$
$(z, y)$	$[\zeta 0 0]$	$[0\zeta\zeta]$	$[\zeta\zeta\zeta]$	$[\zeta\zeta\zeta]$
$(z, x)$	$[\zeta 0 0]$	$[0\zeta\zeta]$	$[\zeta\zeta\zeta]$	$[\zeta\zeta\zeta]$
$(y, x)$	$[0\zeta 0]$	$[\zeta 0\zeta]$	$[\zeta\zeta\zeta]$	$[\zeta\zeta 1-\zeta]$

that the only nonzero elements are given by

$$F_x = (1/N) \left| \left\langle \sum_i S_i^x \exp(-i\mathbf{Q} \cdot \mathbf{r}_i) \right\rangle \right|^2$$

and

$$F_y = (1/N) \left| \left\langle \sum_i S_i^y \exp(-i\mathbf{Q} \cdot \mathbf{r}_i) \right\rangle \right|^2.$$

When the transformation to Fourier coordinates (A3) is used the result is

$$F_x^\pm = \frac{1}{2} S \{ a_1(-\mathbf{q}) + a_1^\dagger(\mathbf{q}) \pm [a_2(-\mathbf{q}) + a_2^\dagger(\mathbf{q})] \}^2$$

and

$$F_y^\pm = \frac{1}{2} S \{ a_1(-\mathbf{q}) - a_1^\dagger(\mathbf{q}) \pm [a_2^\dagger(\mathbf{q}) - a_2(-\mathbf{q})] \}^2,$$

where the upper sign is to be taken when

$$\mathbf{r}_{12} \cdot (\mathbf{Q} - \mathbf{q}) = 2\pi,$$

and the lower when

$$\mathbf{r}_{12} \cdot (\mathbf{Q} - \mathbf{q}) = \pi,$$

where  $\mathbf{r}_{12}$  is the vector distance between spins 1 and 2. Using Eq. (A8), we then find that the mode with frequency  $\omega_1(\mathbf{q})$  has structure factors (omitting population factors)

$$\begin{aligned} F_x^+ &= [S/2\hbar\omega_1(\mathbf{q})][\theta(B+C)\alpha_1 - \beta_1]^2, \\ F_y^- &= [S/2\hbar\omega_1(\mathbf{q})][\theta(B+C)\alpha_1 + \beta_1]^2, \\ F_x^- &= F_y^+ = 0. \end{aligned} \quad (3.11)$$

For the mode with frequency  $\omega_2(q)$ , the results are

$$\begin{aligned} F_x^- &= [S/2\hbar\omega_2(\mathbf{q})][\theta(B-C)\alpha_2 - \beta_2]^2, \\ F_y^+ &= [S/2\hbar\omega_2(\mathbf{q})][\theta(B-C)\alpha_2 + \beta_2]^2, \\ F_x^+ &= F_y^- = 0. \end{aligned} \quad (3.12)$$

The expression for  $\alpha_j$ ,  $\beta_j$ , and  $\theta(x)$  are given in Eq. (A9):

$$\begin{aligned} \alpha_j &= [A + \hbar\omega_j(\mathbf{q})]^{1/2}, \\ \beta_j &= [A - \hbar\omega_j(\mathbf{q})]^{1/2}, \\ \theta(x) &= x/|x|. \end{aligned} \quad (3.13)$$

The relative intensities of the scattering from the different modes are then given by

$$f(\mathbf{Q})^2 (F_x^\pm Q_x^2 + F_y^\pm Q_y^2).$$

## IV. INTERPRETATION OF EXPERIMENTAL RESULTS

### 1. Domain Structure

The main difficulty in obtaining the exchange and anisotropy constants of a model of  $\text{UO}_2$  from the experimental measurements described in Sec. II arises from the multidomain structure of the specimen. Thus the measurements are the sum of the scattering from all domains, and our first problem is then to assign the results as far as possible to the appropriate domains.

There are six different orientations of the domains in the specimen; these will be specified by the notation  $(\alpha, \beta)$ , where  $\alpha$  is the direction perpendicular to the ferromagnetic sheets and  $\beta$  is the spin direction. The domain whose spin waves were discussed in the previous section is then labelled  $(X, Z)$ . Initially, we shall convert the experimental results into results for a single  $(X, Z)$  domain by changing the wave vectors appropriately. These transformations are given in Table III. From this table, it is seen that experimental results in the multidomain crystal, along  $[00\zeta]$  for example, enable us to deduce the dispersion relations along all three cube axes of a single domain specimen. The difficulty lies in the identification of the particular direction for each branch of these results.

It would be of considerable assistance if this separation could be performed with the aid of the neutron-scattering structure factors. However, the requirement that the wave-vector transfer be perpendicular to the vector  $\mathbf{F}$  of the structure factor (Sec. III) together with the multidomain character of the specimen result in the conclusion that all of the modes are observable in an experiment in a  $(1\bar{1}0)$  plane. Of course, some have larger scattering intensities than others, but these can only be compared with experiment once a model has been found for the spin waves. Such a comparison will be discussed later. These conclusions are in agreement with the experimental observation that the intensity of the scattering from the spin waves is largely independent of the wave-vector transfer  $\mathbf{Q}$ , used to study any particular wave vector  $\mathbf{q}$  in the Brillouin zone, except when the branch clearly has a strong phonon component.

Some indications of the domains can be obtained from the symmetry of the experimental results. In the  $[00\zeta]$  direction, the domains  $(Z, X)$  and  $(Z, Y)$  have a Brillouin-zone boundary at the point  $\mathbf{q} = (0, 0, 0.5)$ , and the dispersion relations belonging to these domains must consequently be symmetric about this point. This is clearly not the case for the branch  $A_1$  of Fig. 4. This branch must then be assigned to the other domains, and the frequency of 0.57 at  $\mathbf{q} = (0, 0, 1.0)$  is a zone boundary mode frequency for the  $[0\zeta 0]$  direction (or equivalently the  $[00\zeta]$  direction) of the  $(X, Z)$  domain. Similar conclusions can be derived about the branches observed in the  $[\zeta\zeta 0]$  direction.

A comparison of the results in the  $[\zeta\zeta\zeta]$  and  $[\zeta\zeta 1-\zeta]$

directions also enables us to identify the lowest branch of the  $[\zeta \zeta 1-\zeta]$  direction  $A_4$  as belonging to the  $[\zeta \zeta 1-\zeta]$  or  $[\zeta 1-\zeta \zeta]$  directions in the  $(X, Z)$  domain. This then confirms our assignment of a  $[00\zeta]$  zone boundary frequency.

Further difficulties are created by the magnon-phonon interaction.<sup>10</sup> In order to deduce exchange and anisotropy parameters for the spin waves, it would be convenient to turn off the magnon-phonon interaction, and then to treat it later as a weak perturbation. It is difficult to do this because it is not possible to decide on the influence of the phonons on the magnons unambiguously. In Fig. 4, the phonon lines calculated on the basis of a model for the phonon spectra at 296°K<sup>3</sup> are shown. The results strongly suggest that curve  $B_1$  in the  $[00\zeta]$  direction and curve  $A_3$  in the  $[\zeta \zeta \zeta]$  direction are of strongly phononlike character. This is borne out experimentally, because their intensity, for a given  $\mathbf{q}$ , is very different at different momentum transfers  $\mathbf{Q}$ , as expected for these phonon branches. In the remainder of this section, we describe two attempts to construct models using these various pieces of information to sort out the experimental results.

## 2. Model A (Doubly Degenerate Dispersion Curves)

In view of the number of dispersion curves observed experimentally for a total of six different domains, and the added complications arising from the interaction with the phonons, we attempted to fit the experimental results by a model (A) for which the anisotropy constant  $K_2$  is set to zero. The frequencies  $\omega_1(\mathbf{q})$  and  $\omega_2(\mathbf{q})$  are then equal, giving rise to only one doubly degenerate mode for each wave vector  $\mathbf{q}$ .

The first difficulty this approach meets is to explain the two frequencies at  $\mathbf{q}=0$ . This is overcome by assuming that the upper frequency arises largely from the interaction with the  $[00\zeta]$  zone boundary phonon (the  $[00\zeta]$  zone boundary is a lattice point for the  $(Z, X)$  and  $(Z, Y)$  domains) and that the lower frequency is the predominantly magnetic excitation. There is only one curve,  $A_1$ , which connects this frequency to the lowest frequency of 0.57 (10<sup>12</sup> cps), and hence the exchange interactions of the  $(X, Z)$  model must have at least approximately cubic symmetry about the  $X$  axis. Consequently, we take  $J_2=J_3$  and  $J_5=J_6$  so that the frequencies of modes propagating along  $[00\zeta]$  and  $[0\zeta 0]$  are equal. The identification of the modes observed, Fig. 4, along  $[00\zeta]$  is then, for an  $(X, Z)$  domain:

$A_1$  is a magnon  $[00\zeta]$  branch.  $B_1$  is  $\Delta_5$  phonon branch for small  $\zeta$  and a magnon  $[\zeta 00]$  branch at large  $\zeta$ .  $C_1$  is of  $\Delta_5$  phonon character at both ends and magnetic-like in the middle of the branch.

In the  $[\zeta \zeta 0]$  direction, the identification is the following:

$A_2$  is a  $[\zeta \zeta 0]$  magnon branch.  $B_2$  is a  $[0\zeta \zeta]$  magnon

branch.  $C_2$  is a transverse phonon branch ( $\Sigma_4$ ) which is polarized perpendicular to the  $(1\bar{1}0)$  mirror plane.

In the  $[\zeta \zeta \zeta]$  and  $[\zeta \zeta 1-\zeta]$  directions, the identifications are the following:

$A_3$  is a  $\Lambda_3$  phonon mode at small  $\zeta$  and of  $[\zeta \zeta \zeta]$  magnon character at large  $\zeta$ .  $B_3$  and  $B_4$  are  $[\zeta \zeta \zeta]$  magnon-like for small  $\zeta$ , and of  $\Lambda_3$  phonon character for large  $\zeta$ .  $C_3$  and  $C_4$  arise from the  $[\zeta \zeta 1-\zeta]$  phonon modes.  $\Sigma_2$  denotes a branch of phonons polarized perpendicular to the  $(1\bar{1}0)$  mirror plane.  $A_4$  is the  $[\zeta \zeta 1-\zeta]$  magnon branch.

The parameters of the models were found by least-squares fitting to the magnon part of the experimental results. The parameters of two models, AA and BB, are listed in Table IV, and the frequencies of one of these AB compared with experiment in Fig. 4. The agreement with the experimental results is reasonable, although there are quite striking discrepancies in some regions of reciprocal space particularly near  $\mathbf{q}=(0.5, 0.5, 0)$ .

The main difficulties of this type of theory are the following:

(1) Allen<sup>11</sup> has shown that the  $\mathbf{q}=0$  modes are not split in the infrared spectrum when a magnetic field is applied, and hence concludes they are not doubly degenerate. This contradicts the model.

(2) Many of the branches observed in the neutron-scattering experiments are identified as phonons polarized perpendicular to the  $(1\bar{1}0)$  plane.  $C_2$ ,  $C_3$ , and  $C_4$  are examples of this. The small  $\zeta$  region of  $C_1$  is observed in experiments where the phonon-scattering cross section is zero. Although there will be some intensity from the interaction with the magnons, it seems unlikely that this would be large enough to be consistent with the experimental results.

(3) In the  $[00\zeta]$  direction, the measured curves  $B_1$  and  $C_1$  show a magnon-phonon interaction. However, since the magnon curve there is present in only two of the six domains, an undistorted phonon spectrum would be expected in the other four domains. The experimental results, which are shown in Ref. 10, showed no sign of an undisturbed phonon branch.

(4) Model AA violates the stability criteria (3.5) and (3.6), while the molecular-field estimates of  $T_N$  and  $\theta$  are  $37 \pm 5$  and  $-125 \pm 5$ , whereas the experimental values are 30.8 and  $-200^\circ\text{K}$ .<sup>21</sup> Model AB, on the other hand, satisfies all the stability criteria but gives values of  $T_N$  and  $\theta$  of  $8.5 \pm 10$  and  $-96 \pm 10^\circ\text{K}$ , respectively.

## 3. Model B (Nondegenerate Dispersion Curves)

Since Allen<sup>11</sup> has shown that the magnetic modes are probably nondegenerate at  $\mathbf{q}=0$ , a more satisfactory

<sup>21</sup> A. Arrott and J. E. Goldman, Phys. Rev. **108**, 948 (1957).

TABLE IV. The values of the exchange and anisotropy parameters for various models of  $\text{UO}_2$ .  $J_1, J_2, J_3$  and  $J_4$  are for nearest neighbors,  $J_5, J_6$  next nearest, and  $K_1$  and  $K_2$  anisotropy constants. The units are  $10^{-3}$  eV.  $\chi$  is the ratio of the mean deviation of the calculated frequencies of the model to the experimental error.

Model	$J_1$	$J_2$	$J_3$	$J_4$	$J_5$	$J_6$	$K_1$	$K_2$	$\chi$
AA	$-1.44 \pm 0.05$	$-1.31 \pm 0.08$	$= J_2$	0	0	0	$1.95 \pm 0.65$	0	6.50
AB	$-1.15 \pm 0.08$	$-0.84 \pm 0.16$	$= J_2$	$-0.17 \pm 0.04$	$= J_4$	$= J_4$	$2.56 \pm 0.65$	0	5.42
BA	$-0.20 \pm 0.06$	$0.06 \pm 0.02$	$-0.21 \pm 0.08$	0	0	0	$11.2 \pm 3.1$	$20.25 \pm 6.9$	3.65
BB	$-0.33 \pm 0.03$	$0.16 \pm 0.04$	$-0.54 \pm 0.12$	$-0.06 \pm 0.02$	$= J_4$	$= J_4$	$6.45 \pm 0.8$	$8.8 \pm 2.07$	3.09
BC	$-0.26 \pm 0.15$	$0.10 \pm 0.09$	$-0.33 \pm 0.29$	$-0.04 \pm 0.05$	$-0.06 \pm 0.03$	$-0.01 \pm 0.04$	$8.6 \pm 5.2$	$14.2 \pm 12.4$	3.09

model than model A must take this into account. This is done by allowing the second anisotropy parameter  $K_2$  to be nonzero. There are then two dispersion curves for each domain, giving rise to a very large number of branches in all. The first difficulty in the use of a model of this type is, then, to reduce the number of dispersion curves as far as possible. As will be discussed below, it is found that in each domain one of the branches had a considerably larger structure factor than the other in the  $(1\bar{1}0)$  plane. In view of this, the experimental results were fitted as far as possible to those modes with a large structure factor, and the other modes were given much less statistical weight in the fitting process.

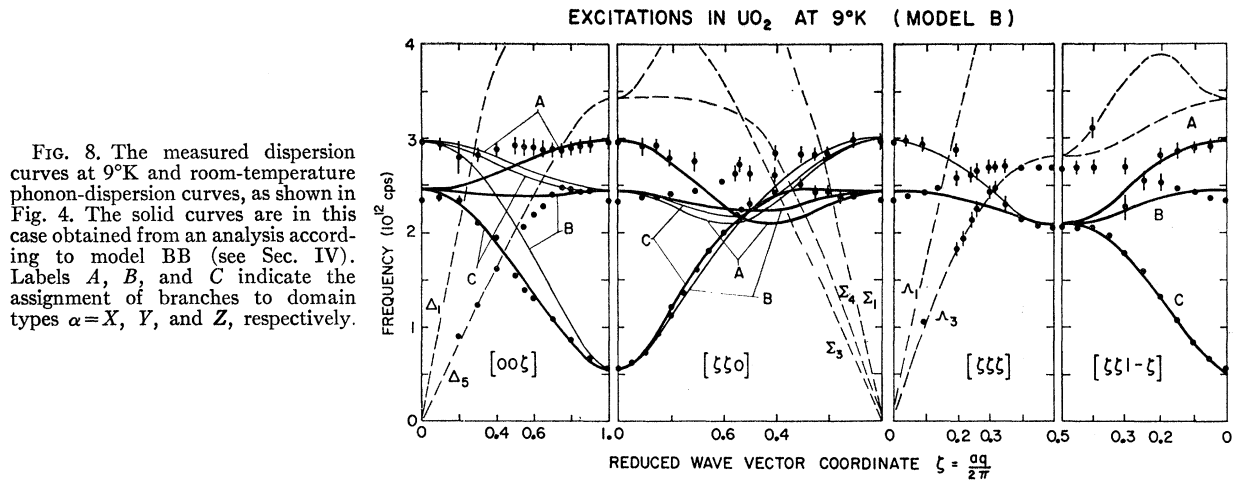
The third difficulty of model A can only be overcome if all the domains have branches with a frequency of about  $2.40 \times 10^{12}$  cps at the point  $\mathbf{q} = (0, 0, 1.0)$ . This inevitably leads to the use of a model for which all the exchange constants are different.

The assignment of the large structure factor branches to the  $(X, Z)$  domain is then as follows: in the  $[\zeta 00]$  direction from the low  $\zeta$  region of  $A_1$  (Fig. 4) to the  $\zeta = 1$  region of  $C_1$ , in the  $[00\zeta]$  direction from the low  $\zeta$  region of  $A_1$  to the  $\zeta = 1$  region of  $B_1$ , and in the  $[0\zeta 0]$  direction  $A_1$ . The  $[0\zeta\zeta]$  direction modes are given by  $C_2$ , the  $[\zeta\zeta 0]$  direction by  $B_2$ , and the  $[\zeta 0\zeta]$  direction by  $A_2$ . The large structure factor mode in the  $[\zeta\zeta\zeta]$  direction is given by the low  $\zeta$  region of  $B_3$  and large  $\zeta$  region of  $A_3$ , and in the  $[\zeta\zeta 1 - \zeta]$  direction by the low  $\zeta$  region of  $B_4$  and the  $[\zeta 1 - \zeta\zeta]$  direction by  $A_4$ . The low  $\zeta$  regions of the modes  $C_1, C_2$ , and  $C_3$  are then not observed because they belong to the weak structure factor modes, and the large  $\zeta$  end of  $C_3$  and  $C_4$  are TA phonon modes. The results of fitting the parameters of the model to this assignment of the branches is shown in Table IV. One of these models, BB, is compared with the experimental results in Fig. 8.

The fitting errors for the B models in the table are not comparable with those of the A models, because of the changes in the assignments of the modes. In Fig. 8, the modes with large structure factors are shown by thick lines; those with weak structure factors by thin lines; and the phonons by dashed lines. The magnetic branches are labelled to give the domains. The agreement with experiment shown in Fig. 8 is reasonable. The main discrepancies occur in the  $[00\zeta]$  direction, where a strong mode from the  $(X, Z)$  and  $(Y, Z)$  domains was not observed in the experiments, and in the region  $\mathbf{J} = (0.5, 0.5, 0)$ , where the calculated modes have lower frequencies than the experimental ones.

These models do not give good agreement for the transition temperature and Curie temperature. For models BA, BB, BC, respectively,  $T_N$  is  $-2.1, -1.3$ , and  $-2.7^\circ\text{K}$ , while  $\theta$  is  $-10.7, -26$ , and  $-18^\circ\text{K}$ . The stability criteria (3.5) are violated by all these models, but they satisfy the other criteria.

The reduced neutron-scattering cross sections (3.11) and (3.12) have been calculated, and the results for



model BB are shown in Fig. 9. The intensities can be deduced from these curves by considering the component of  $F$  perpendicular to the wave-vector transfer  $Q$ . Unfortunately, a detailed comparison of these calculations with experiment is not possible, because it is by

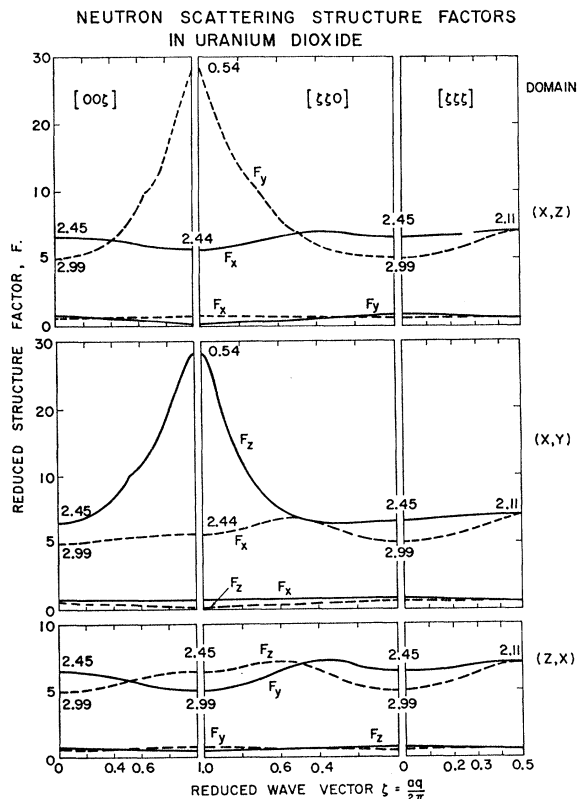


FIG. 9. Reduced structure factors  $F$  governing the neutron cross sections for one-magnon scattering processes, as computed from model BB. The scale is arbitrary, but note the scale change at 10 units. The calculated magnon frequency (in units of  $10^{12}$  cps) appropriate to each branch is shown at zone boundaries and zone center. The dotted lines correspond to  $F^-$  components and solid lines to  $F^+$  components.

no means certain that the specimen had a completely random arrangement of domains, and the relative intensities are clearly dependent on this arrangement. There is also the possibility of spurious double-scattering processes.<sup>15</sup> Finally, the spin direction in the ferromagnetic sheets is unknown. In Sec. III, we assumed it to be along a cube axis; and although the frequencies are not altered if it were along a different direction, the cross sections would be. In spite of all these uncertainties, many of the calculated intensities are in qualitative agreement with experiment.

Allen<sup>11</sup> has used a model with one anisotropy constant but has then split the degeneracy of the modes by using an anisotropic exchange interaction between nearest neighbors. There are two parameters describing the exchange and one for the anisotropy; he obtains these from his infrared measurements. This model overcomes difficulty 1 of our models of type A, but still leaves difficulties 2 and 3.

None of the models are completely satisfactory, possibly because the exchange interactions are far more complex than assumed here, or because our assignment of the experimental results is incorrect. However, more complicated fits were attempted in which the nearest-neighbor exchange constants were assumed to be anisotropic and specified by parameters  $J_{xx}, J_{yy},$  and  $J_{zz}$ . No improvement in the fit was obtained with these models. Undoubtedly experiments on a single domain crystal of  $UO_2$  would be of considerable assistance in clarifying these points.

## V. MAGNON-PHONON INTERACTION

### 1. Origin of the Magnon-Phonon Interaction

The experimental results described in Sec. II and earlier<sup>10</sup> show that in uranium dioxide there is a strong interaction between the magnetic and phonon excitations. This was unexpected, because no structure change has been observed at the antiferromagnetic phase transition, and also because measurements on other anti-

ferromagnetic materials,  $\text{MnF}_2$ ,<sup>2</sup>  $\text{RbMnF}_3$ ,<sup>22</sup>  $\text{KMnF}_3$ ,<sup>23</sup> and  $\text{CoF}_2$ <sup>24</sup> have failed to show any magnon-phonon interaction. This is in spite of the fact that the magnetic electrons are situated at the edge of the ions in the  $3d$  shell, but are buried well within the ion in the  $5f$  shell of uranium.

The origin of these effects may be that in  $\text{Mn}^{2+}$  ions the electronic configuration is an  $s$  state and is largely unaffected by the crystalline field. Consequently, the motion of the ions will not split the ground state but only modify the exchange parameters. These modifications result in contributions to the Hamiltonian proportional to  $S_i^\alpha S_j^\beta u_\gamma(lk)$ , which gives rise only to comparatively small lifetimes and shifts, as described by Upadhyaya and Sinha.<sup>25</sup> [ $\mathbf{u}(lk)$  is the displacement of the  $k$ th atom in  $l$ th unit cell.] In  $\text{CoF}_2$ , the ground state is a Kramers doublet which also cannot be split by any changes in the crystalline field.

On the other hand, in  $\text{UO}_2$ , the ground state is a triplet which can be split by a change in the crystalline field due to the motion of the ions. Consequently, there will be terms in the Hamiltonian proportional to  $S_i^\alpha u_\beta(lk)$  which give rise to the much larger effects of the type observed in  $\text{UO}_2$ . These considerations suggest that a large magnon-phonon interaction will occur whenever the ground state may be split by the crystalline field resulting from the motion of the ions.

The theory of the interaction between magnons and phonons at short wavelengths has been discussed by Lord,<sup>26</sup> starting from a phenomenological form for the magnetoelastic part of the Hamiltonian. We shall deduce a form from first principles. The displacement of an ion of type  $k$  in the  $l$ th unit cell,  $\mathbf{u}(lk)$ , gives rise to an electric dipole which sets up an electric field at all the magnetic ions. The potential at a distance  $\mathbf{R}$  from a dipole  $\mathbf{p}(lk)$  is

$$V(lk) = \mathbf{p}(lk) \cdot \mathbf{R} / |\mathbf{R}|^3.$$

If the equilibrium distance between the ion ( $lk$ ) and a magnetic ion is  $\mathbf{R}_0$ , the field over the magnetic ion can be obtained by writing  $\mathbf{R} = \mathbf{R}_0 + \mathbf{v}$ , where  $\mathbf{v}$  is the vector specifying the unpaired electron coordinates within the magnetic ion. Expanding the potential to first order in  $\mathbf{v}$  leads to

$$V(lk) = [\mathbf{p}(lk) \cdot \mathbf{v} / |\mathbf{R}_0|^3] - \{3[\mathbf{p}(lk) \cdot \mathbf{R}_0](\mathbf{R}_0 \cdot \mathbf{v}) / |\mathbf{R}_0|^5\}. \quad (4.1)$$

This term is linear in  $\mathbf{v}$  and consequently does not contribute within any one configuration of the ion and can only mix different configurations.<sup>27</sup> Its contribution

<sup>22</sup> C. G. Windsor and R. W. H. Stevenson, Proc. Phys. Soc. (London) **87**, 501 (1966).

<sup>23</sup> S. J. Pickart, M. F. Collins, and C. G. Windsor, J. Appl. Phys. **37**, 1054 (1966).

<sup>24</sup> R. A. Cowley, P. C. Martel, and R. W. H. Stevenson, Phys. Rev. Letters **18**, 162 (1967).

<sup>25</sup> U. N. Upadhyaya and K. P. Sinha, Phys. Rev. **130**, 939 (1963).

<sup>26</sup> A. E. Lord (private communication).

<sup>27</sup> W. Low, in *Solid State Physics*, edited by F. Seitz and D. Turnbull (Academic Press Inc., New York, 1960), Suppl. 2.

is probably small, therefore. The second-order term is

$$V(lk) = -\{3[\mathbf{p}(lk) \cdot \mathbf{v}](\mathbf{R}_0 \cdot \mathbf{v}) / |\mathbf{R}_0|^5\} - \frac{3}{2}\{[\mathbf{p}(lk) \cdot \mathbf{R}_0](\mathbf{v} \cdot \mathbf{v}) / |\mathbf{R}_0|^5\} + \frac{1}{2}\{[\mathbf{p}(lk) \cdot \mathbf{R}_0](\mathbf{R}_0 \cdot \mathbf{v})^2 / |\mathbf{R}_0|^7\}. \quad (4.2)$$

Within any manifold with  $J$  constant, the vector  $\mathbf{v}$  can be replaced by its operator equivalent to yield an interaction given by

$$V = \frac{3}{2}\alpha_J \langle r^2 \rangle \sum_{lk} (1 / |\mathbf{R}_0(lk)|^5) \times ([\mathbf{p}(lk) \cdot \mathbf{R}_0(lk)] \{5[\mathbf{J} \cdot \mathbf{R}_0(lk)]^2 / |\mathbf{R}_0(lk)|^2 - \mathbf{J} \cdot \mathbf{J}\} - 2[\mathbf{p}(lk) \cdot \mathbf{J}][\mathbf{R}_0(lk) \cdot \mathbf{J}]), \quad (4.3)$$

where  $\alpha_J$  is a constant given by Low<sup>27</sup> and  $\langle r^2 \rangle$  the average radius squared of the magnetic electronic distribution. This expression then enables us to evaluate the magnon-phonon interaction explicitly.

## 2. Magnon-Phonon Interaction in $\text{UO}_2$

In the case of  $\text{UO}_2$ , it is possible to simplify further the expression for the magnetoelastic Hamiltonian (4.3) by replacing the coordinate  $\mathbf{J}$  with the effective spin  $\mathbf{S}$  in the ground-state triplet. Furthermore, we shall restrict the interaction for each magnetic ion to nearest-neighbor oxygen ions. This approximation is neither necessary nor very satisfactory, since the potential (4.2) falls off only as  $1/R^4$ , but it is probably at least of semiquantitative value and greatly decreases the amount of numerical work needed. The nearest-neighbor oxygen ions are placed at  $(\epsilon_x, \epsilon_y, \epsilon_z)a/4$ , where  $\epsilon_{x,y,z} = \pm 1$ . The electric dipole  $\mathbf{p}(lk) = Z_k \mathbf{u}(lk)$ , where  $Z_k$  is the effective charge of the ion, and hence the interaction with one particular oxygen ion is

$$K \mathbf{u}(lk) \cdot \boldsymbol{\epsilon}(lk) \{ \frac{8}{3} [\mathbf{S} \cdot \boldsymbol{\epsilon}(lk)]^2 - \mathbf{S} \cdot \mathbf{S} \} - 2K [\mathbf{u}(lk) \cdot \mathbf{S}] [\boldsymbol{\epsilon}(lk) \cdot \mathbf{S}], \quad (4.4)$$

where  $\boldsymbol{\epsilon}(lk)$  is the vector  $\epsilon_x, \epsilon_y, \epsilon_z$ , and

$$K = \frac{1}{2}\sqrt{3}[\alpha_J / |\mathbf{R}_0(lk)|^4] \langle r^2 \rangle (2-g)^2 e^2 Z_k.$$

In the ordered structure, the spin is aligned along  $S^z$ , and expression (4.4) can be evaluated for this static structure. The result is

$$K \mathbf{u}(lk) \cdot \boldsymbol{\epsilon}(lk) [\frac{8}{3} (S^z)^2] - 2K (S^z)^2 \boldsymbol{\epsilon}(lk) u_z(lk). \quad (4.5)$$

In order to evaluate the total force on the oxygen ion ( $lk$ ) due to the ordering of the spins, this expression must be summed over all the magnetic neighbors of ( $lk$ ). These are  $\boldsymbol{\epsilon}(lk) = (1, 1, 1)$  and  $(-1, -1, 1)$ , with  $S^z$  negative. The resultant total force on the oxygen ions is then zero, in agreement with the failure to observe any change of the structure at the phase transition by diffraction techniques.

The most interesting terms from Eq. (4.4) are those that involve a single spin-wave operator. These are obtained by the formalism of Sec. III from those which

contain a single  $S^z$  in them, namely,

$$V(lk) = \frac{1}{3}KS^z\epsilon_z(lk) \{4u_x(lk)S^z + 4u_y(lk)S^y + 10\epsilon_y(lk)\epsilon_x(lk)[u_x(lk)S^y + u_y(lk)S^z]\} + \frac{4}{3}KS^zu_z(lk)[\epsilon_x(lk)S^z + \epsilon_y(lk)S^y]. \quad (4.6)$$

The magnetoelastic Hamiltonian is then obtained by summing this expression over all ions ( $lk$ ) for the nearest-neighbor oxygen ions. It is easily shown that this expression then satisfies the condition of translational invariance because

$$\sum_{lk} \epsilon_\alpha(lk) = 0.$$

The calculation is completed by transforming to magnon and phonon coordinates. The former are described in Sec. III, and the latter are given by

$$\mathbf{u}(lk) = \sum_{\mathbf{q}j} [\hbar/2N\omega_p(\mathbf{q}j)]^{1/2} \mathbf{e}(k | \mathbf{q}j) \times \exp[i\mathbf{q} \cdot \mathbf{R}(lk)] A(\mathbf{q}j), \quad (4.7)$$

where  $\omega_p(\mathbf{q}j)$  is the ( $\mathbf{q}j$ ) phonon frequency and  $\mathbf{e}(k | \mathbf{q}j)$  the eigenvector of the  $k$ th ion in that mode. The phonon creation and destruction operators are written  $A(\mathbf{q}j) = a^\dagger(\mathbf{q}j) - a(-\mathbf{q}j)$ . When Eq. (4.7) is substituted into (4.6) and the resultant summed over all the magnetic ions  $k$ , we obtain terms

$$\sum_{\mathbf{q}jj'} V(\mathbf{q}jj') A(\mathbf{q}j) B(\mathbf{q}j'), \quad (4.8)$$

where for magnon mode (1)

$$B(\mathbf{q}1) = b_1(-\mathbf{q}) - \theta(B+C)b_1^\dagger(\mathbf{q}),$$

and

$$V(\mathbf{q}j1) = \frac{1}{3} \sum_{l'k'} KS(S/\hbar)^{1/2} [\omega_p(\mathbf{q}j)\omega_1(\mathbf{q})]^{-1/2} \times \{ \epsilon_z(l'k') [2e_y(k' | \mathbf{q}j) + 5\epsilon_x(l'k')\epsilon_y(l'k')e_x(k' | \mathbf{q}j)] + 2\epsilon_y(l'k')e_z(k' | \mathbf{q}j) \} \exp[i\mathbf{q} \cdot \mathbf{R}(l'k', 0k)] \times [\alpha_1 + \theta(B+C)\beta_1].$$

Similarly, for magnon mode (2),

$$B(\mathbf{q}2) = b_2^\dagger(\mathbf{q})\theta(B-C) - b_2(-\mathbf{q})$$

and

$$V(\mathbf{q}j2) = \frac{1}{3} \sum_{l'k'} KS(S/\hbar)^{1/2} [\omega_p(\mathbf{q}j)\omega_2(\mathbf{q})]^{-1/2} \times \{ \epsilon_z(l'k') [2e_x(k' | \mathbf{q}j) + 5\epsilon_x(l'k')\epsilon_y(l'k')e_y(k' | \mathbf{q}j)] + 2\epsilon_x(l'k')e_z(k' | \mathbf{q}j) \} \exp[i\mathbf{q} \cdot \mathbf{R}(l'k', 0k)] \times [\alpha_2 - \theta(B-C)\beta_2].$$

The operators  $b$  and coefficients  $\alpha$ ,  $\beta$ ,  $\theta$ , etc., are defined in Sec. III. These expressions then enable us to reduce the combined magnon-phonon frequencies in terms of the coefficients  $K$ . The easiest procedure is to write the equations of motion for the operators  $b(-\mathbf{q})$ ,  $b^\dagger(\mathbf{q})$ ,  $a(-\mathbf{q}j)$ , and  $a^\dagger(\mathbf{q}j)$  in a manner similar to that used to deduce the magnon frequencies in the appendix. The two frequencies are then given for mag-

non mode  $j'$  and phonon mode  $j$  by the equation

$$\omega^2 = \frac{1}{2}(\omega_M^2 + \omega_p^2) \pm \frac{1}{2}(\omega_M + \omega_p)[(\omega_M - \omega_p)^2 + 4(V/\hbar)^2]^{1/2},$$

where

$$\omega_M = \omega_{j'}(\mathbf{q})$$

$$\omega_p = \omega_p(\mathbf{q}j),$$

and

$$V = V(\mathbf{q}jj').$$

The splitting between two modes that are degenerate in the absence of the interaction is then

$$2V(\mathbf{q}jj') \quad (4.9)$$

if  $V(\mathbf{q}jj') < \omega_p(\mathbf{q}j)$ .

### 3. Numerical Calculations

Numerical calculations of the magnon-phonon interaction coefficients have been made using this model which considers the interaction of the magnetic electrons with the nearest-neighbor rigid oxygen ions. The models for the magnon spectra described above were used for the magnon variables and model III of Dolling *et al.*<sup>3</sup> for the phonon modes. The parameter  $\langle r^2 \rangle$  of the electron distribution of the magnetic electrons was obtained from the calculations of Satten *et al.*<sup>28</sup>

The results show that the magnon-phonon interaction is largest near the  $[00\xi]$  and  $[\xi\xi\xi]$  zone boundaries and with the transverse phonon modes. This is in good agreement with the experiment results. The interaction with the longitudinal modes is calculated to be weaker than with the transverse modes, except in the  $[\xi\xi0]$  direction. The complete calculations of the coupled magnon-phonon dispersion relation have not been made but a comparison can be made for the two clear examples of the interaction observed experimentally: In the  $[\xi\xi\xi]$  direction, the splitting between the modes is observed to be  $0.22 \pm 0.05$ , and that calculated is 0.28 for model BB. In the  $[00\xi]$  direction, the situation is more complicated because of the large number of different interaction coefficients for the different domains. However, the calculations yield on average 0.26, while experimentally the splitting is  $0.4 \pm 0.05$ . These results show quite a remarkable agreement between experiment and calculation for such a simple model. More refined calculations would need to take account of more distant neighbors, screening of the 5f electrons by outer electrons, the effective charge of the oxygen ions, covalent bonding, and many of the other imperfections in this model. Clearly, the results do show, however, that the mechanism of the interaction proposed here is essentially correct.

The calculations also show an interaction between the ( $Z, X$ ) domain magnons and phonons at the  $[00\xi]$  zone boundary. Since this is a magnetic lattice point, it gives rise to a mechanism by which the transverse acoustic mode is observable in the infrared spectrum, as found by Allen.<sup>11</sup>

<sup>28</sup> R. A. Satten, C. L. Schrieber, and E. Y. Wong, J. Chem. Phys. **42**, 162 (1965).

Similar calculations have been made for the type A magnon models, AA and AB. In these cases, the phonon interaction splits the degeneracy of the magnon branches giving rise to two branches in each direction. This arises because the phonon introduces a crystal-field distortion of low symmetry. Although the actual numerical results differ from those of model BB, the results are very similar in magnitude.

## VI. SUMMARY

The dispersion relation for magnetic excitations in antiferromagnetic uranium dioxide has been measured at very low temperatures by neutron inelastic scattering methods; the temperature dependence of selected modes has also been investigated, particularly near the Néel temperature. The results and subsequent theoretical analysis show that the magnetic interactions in  $\text{UO}_2$  are considerably more complex than those in several other antiferromagnets whose magnon spectra have been studied, and also that there is a strong magnon-phonon interaction which arises because the triplet ground state of the  $\text{U}^{4+}$  ion may be split by distortions of the crystal field produced by phonons.

A few comments regarding the validity of Blume's theory<sup>9</sup> for  $\text{UO}_2$  may be useful at this point. An important postulate of this theory is that in the paramagnetic phase the  $\Gamma_1$  singlet lies just below the  $\Gamma_{25'}$  triplet. In the antiferromagnetic phase, the triplet is split by the internal field generated by the magnetic order, and the lowest of these three states is then below the  $\Gamma_1$  level. The first-order character of the transition is readily visualized as the thermal excitation of electrons into the nonmagnetic  $\Gamma_1$  level that reduces the triplet splitting, thus increasing the  $\Gamma_1$  population, and so on. The two most prominent lines in the infrared absorption spectra are then interpreted as triplet-singlet transitions,<sup>13</sup> even though the transition probabilities for such transitions would be expected to be very low.<sup>11</sup> The corresponding neutron groups observed in our experiments were similarly much more intense than would be expected on this basis. The large scattering cross section of the low-frequency mode ( $0.57 \times 10^{12}$  cps) which exhibits a strong temperature dependence near the transition point would appear to be inconsistent with Blume's theory.

In this paper, we have adopted the approach of Rahman and Runciman,<sup>8</sup> that the  $\Gamma_1$  singlet level is so far above the  $\Gamma_{25'}$  triplet as to play a negligible part in the low-lying excitations of the system. This approach seems adequate for a description of the excitations, including the unusually large magnon-phonon interaction.

The transition in  $\text{UO}_2$  is unusual, however; it appears to be first order,<sup>6</sup> it is associated with an anomaly in the elastic constants,<sup>29</sup> and the temperature dependence of the magnons is surprisingly weak. These properties

<sup>29</sup> O. G. Brandt and C. T. Walker, Phys. Rev. Letters 18, 11 (1967).

are believed to arise from the strong magnon-phonon coupling in  $\text{UO}_2$ .

The lowest triplet state of the uranium ions will tend to be unstable at low temperatures against a distortion of the lattice which splits the degeneracy. The process is that involved in a Jahn-Teller instability.<sup>27</sup> This distortion is undoubtedly very small but could give rise to the unusually large anisotropy constants found in the magnon spectra. It is also comparatively easy to understand the behavior of the elastic constants on this model. A distortion of the structure splits the degeneracy of the triplet, which at low temperature reduces the energy required to produce the distortion until a spontaneous distortion sets in. The phase transition is then a cooperative Jahn-Teller distortion involving not only the Jahn-Teller effect but also the coupling between the magnetic moments. It seems likely that such an approach is capable of explaining the abrupt nature of the phase transition and also the temperature dependence of the magnetic excitations. It is hoped to discuss these matters further in a later publication.

## ACKNOWLEDGMENTS

The authors have benefited from useful discussions with Dr. S. J. Allen, Dr. A. J. Sievers, and Dr. K. Aring and colleagues at Chalk River. They also wish to thank E. A. Glaser, A. Betts, R. Dutkiewicz, and M. McManus for technical assistance and E. Becker for taking some of the data.

## APPENDIX

### Antiferromagnetic Spin-Wave Theory for $\text{UO}_2$

The Hamiltonian for the spin waves in  $\text{UO}_2$  is given by Eq. (3.1) as

$$H = - \sum_{ij} J(ij) \mathbf{S}_i \cdot \mathbf{S}_j - K_1 \sum_i (S_i^z)^2 - K_2 \sum_i [(S_i^x)^2 - (S_i^y)^2]. \quad (\text{A1})$$

The spin direction is taken to be along [001], and the ferromagnetic sheets are perpendicular to [100]. It is convenient to introduce new local axes with the spin direction along (+z). For site 1, these axes coincide with the crystal axes, but for site 2, the transformation is  $x \rightarrow x$ ,  $y \rightarrow -y$ ,  $z \rightarrow -z$ . In terms of the operators  $S^+$  and  $S^-$  referred to these local axes, the Hamiltonian becomes

$$H = -\frac{1}{2} \sum_{ij}^L J(ij) \left[ \frac{1}{2} (S_i^+ S_j^- + S_i^- S_j^+ + 2S_i^z S_j^z) \right] - \frac{1}{2} \sum_{ij}^D J(ij) \left[ \frac{1}{2} (S_i^+ S_j^+ + S_i^- S_j^- - 2S_i^z S_j^z) \right] - K_1 \sum_i (S_i^z)^2 - \frac{1}{2} K_2 \sum_i (S_i^+ S_i^+ + S_i^- S_i^-). \quad (\text{A2})$$

The  $\sum^L$  means summation over all like spins, and  $\sum^D$  means summation over all unlike spins. The spin-wave spectra are then obtained by use of the Holstein-

Primakoff transformation, which in Fourier representation is

$$\begin{aligned} S_i^+ &= (2S/N)^{1/2} \sum_{\mathbf{q}} \exp(-i\mathbf{q} \cdot \mathbf{r}_i) \mathbf{a}_k(\mathbf{q}), \\ S_i^- &= (2S/N)^{1/2} \sum_{\mathbf{q}} \exp(i\mathbf{q} \cdot \mathbf{r}_i) \mathbf{a}_k^\dagger(\mathbf{q}), \\ S_i^z &= S - (1/N) \sum_{\mathbf{q}\mathbf{q}'} \exp[i(\mathbf{q}-\mathbf{q}') \cdot \mathbf{r}_i] a_k^\dagger(\mathbf{q}) a_k(\mathbf{q}'), \end{aligned} \quad (\text{A3})$$

where suffix  $k$  denotes the spin type. When these expressions are substituted into Eq. (A2), the result is a Hamiltonian which can be written as a constant term and a sum of terms dependent upon the wave vector  $\mathbf{q}$ . The partial quadratic Hamiltonian is then

$$\begin{aligned} H_{\mathbf{q}} &= \sum_{kk'} A_{kk'}(\mathbf{q}) [a_k^\dagger(\mathbf{q}) a_{k'}(\mathbf{q}) + a_k(\mathbf{q}) a_{k'}^\dagger(\mathbf{q})] \\ &\quad + B_{kk'}(\mathbf{q}) [a_k^\dagger(\mathbf{q}) a_k^\dagger(-\mathbf{q}) + a_k(\mathbf{q}) a_{k'}(-\mathbf{q})], \end{aligned} \quad (\text{A4})$$

where for our model of  $\text{UO}_2$

$$\begin{aligned} A_{kk'}(\mathbf{q}) &= A = \delta_{kk'} \left\{ - \sum_j^L SJ(0j) [\exp(i\mathbf{q} \cdot (\mathbf{r}_j - \mathbf{r}_0)) - 1] \right. \\ &\quad \left. - S \sum_j^D J(0j) - 2SK_1 \right\}, \end{aligned}$$

$$B_{kk}(\mathbf{q}) = B = -SK_2,$$

$$B_{kk'}(\mathbf{q}) = C = -S \sum_j^D J(0j) \exp[i\mathbf{q} \cdot (\mathbf{r}_j - \mathbf{r}_0)], \quad k \neq k'.$$

The spin-wave operators are linear combinations of the operators  $a_k(\mathbf{q})$  and  $a_k^\dagger(-\mathbf{q})$ , namely,

$$\begin{aligned} b_j^\dagger(\mathbf{q}) &= \sum_k e_1(k, \mathbf{q}j) a_k^\dagger(\mathbf{q}) + \sum_k e_2(k, \mathbf{q}j) a_k(-\mathbf{q}), \\ b_j(-\mathbf{q}) &= \sum_k e_3(k, \mathbf{q}j) a_k^\dagger(\mathbf{q}) + \sum_k e_4(k, \mathbf{q}j) a_k(-\mathbf{q}). \end{aligned}$$

The Hamiltonian (A3) in these new operators is then

$$H_{\mathbf{q}} = \sum_{\mathbf{q}j} \hbar\omega_j(\mathbf{q}) b_j^\dagger(\mathbf{q}) b_j(\mathbf{q}). \quad (\text{A5})$$

The solution for the  $\omega_j(\mathbf{q})$  and for the matrices of coefficients  $e_1, e_2, e_3,$  and  $e_4$  can be deduced by comparing the Heisenberg equations of motion for the  $b$  and  $a$  operators. For the  $b$  operators, the equation is

$$\begin{aligned} [H_{\mathbf{q}}, b_j^\dagger(\mathbf{q})] &= \hbar\omega_j(\mathbf{q}) b_j^\dagger(\mathbf{q}), \\ [H_{\mathbf{q}}, b_j(-\mathbf{q})] &= -\hbar\omega_j(\mathbf{q}) b_j(-\mathbf{q}). \end{aligned}$$

Combining this with the corresponding equation for the  $a$  operators gives the matrix equation

$$\begin{pmatrix} \hbar\omega_j(\mathbf{q}) \mathbf{I} & \\ & -\hbar\omega_j(\mathbf{q}) \mathbf{I} \end{pmatrix} \begin{pmatrix} \mathbf{e}_1 & \mathbf{e}_2 \\ \mathbf{e}_3 & \mathbf{e}_4 \end{pmatrix} = \begin{pmatrix} \mathbf{e}_1 & \mathbf{e}_2 \\ \mathbf{e}_3 & \mathbf{e}_4 \end{pmatrix} \begin{pmatrix} \mathbf{A} & \mathbf{B} \\ -\mathbf{B} & -\mathbf{A} \end{pmatrix}. \quad (\text{A6})$$

This equation shows that the  $\pm \hbar\omega_j(\mathbf{q})$  are the eigenvalues of the matrix

$$\begin{pmatrix} \mathbf{A} & \mathbf{B} \\ -\mathbf{B} & -\mathbf{A} \end{pmatrix}$$

and that the  $\mathbf{e}$ 's are given by the eigenvectors. The requirement that the  $b$  operators should be Bose operators enables us both to distinguish between the different eigenvalues and to normalize the eigenvectors. It is fairly readily shown that these conditions give

$$\sum_k [e_1(k, \mathbf{q}j)^2 - e_2(k, \mathbf{q}j)^2] = 1$$

and

$$\sum_k [e_3(k, \mathbf{q}j)^2 - e_4(k, \mathbf{q}j)^2] = -1.$$

This enables us both to determine the sign of  $\omega_j(\mathbf{q})$  and also to associate the eigenvector with either  $b_j^\dagger(\mathbf{q})$  or  $b_j(-\mathbf{q})$ . In the case of our model of  $\text{UO}_2$ , the matrix is

$$\begin{pmatrix} A & 0 & -B & -C \\ 0 & A & -C & -B \\ B & C & -A & 0 \\ C & B & 0 & -A \end{pmatrix}$$

and the eigenfrequencies are given by

$$\begin{aligned} \hbar\omega_1(\mathbf{q}) &= [A^2 - (B+C)^2]^{1/2}, \\ \hbar\omega_2(\mathbf{q}) &= [A^2 - (B-C)^2]^{1/2}. \end{aligned} \quad (\text{A7})$$

The expressions for the new spin-wave operators are

$$\begin{aligned} b_1^\dagger(\mathbf{q}) &= \frac{1}{2} [\hbar\omega_1(\mathbf{q})]^{-1/2} \{ \theta(B+C) \alpha_1 [a_1^\dagger(\mathbf{q}) + a_2^\dagger(\mathbf{q})] \\ &\quad + \beta_1 [a_1(-\mathbf{q}) + a_2(-\mathbf{q})] \}, \\ b_1(\mathbf{q}) &= \frac{1}{2} [\hbar\omega_1(\mathbf{q})]^{-1/2} \{ \theta(B+C) \beta_1 [a_1^\dagger(\mathbf{q}) + a_2^\dagger(\mathbf{q})] \\ &\quad + \alpha_1 [a_1(-\mathbf{q}) + a_2(-\mathbf{q})] \}, \\ b_2^\dagger(\mathbf{q}) &= \frac{1}{2} [\hbar\omega_2(\mathbf{q})]^{-1/2} \{ \theta(B-C) \alpha_2 [a_1^\dagger(\mathbf{q}) - a_2^\dagger(\mathbf{q})] \\ &\quad + \beta_2 [a_1(-\mathbf{q}) - a_2(-\mathbf{q})] \}, \\ b_2(\mathbf{q}) &= \frac{1}{2} [\hbar\omega_2(\mathbf{q})]^{-1/2} \{ \theta(B-C) \beta_2 [a_1^\dagger(\mathbf{q}) - a_2^\dagger(\mathbf{q})] \\ &\quad + \alpha_2 [a_1(-\mathbf{q}) - a_2(-\mathbf{q})] \}, \end{aligned} \quad (\text{A8})$$

where

$$\begin{aligned} \alpha_j &= [A + \hbar\omega_j(\mathbf{q})]^{1/2}, \\ \beta_j &= [A - \hbar\omega_j(\mathbf{q})]^{1/2}, \end{aligned} \quad (\text{A9})$$

and

$$\theta(x) = x/|x|.$$